Optics Letters

Compact and broadband silicon TE-pass polarizer based on tapered directional coupler

Zakriya Mohammed,[1,*] Bruna Paredes,[2] and Mahmoud Rasras[2]

[1]Electrical and Computer Engineering, New York University- Tandon School of Engineering, Brooklyn, New York 11201, USA
[2]Electrical and Computer Engineering, New York University- Abu Dhabi, Abu Dhabi 129118, United Arab Emirates
*Corresponding author: zm775@nyu.edu

Received 28 February 2022; revised 20 June 2022; accepted 21 June 2022; posted 22 June 2022; published 6 July 2022

We demonstrate a novel TE-pass polarizer, to the best of our knowledge, on a silicon-on-insulator (SOI) platform. The device's working principle is based on the phase-matched coupling of the unwanted TM0 mode in an input waveguide to the TM1 mode in a tapered directional coupler (DC), which is then guided through a low-loss bend (180-degree) and scattered in a terminator section with low back reflections. However, the input TE0 mode is routed through the tapered section uncoupled with negligible loss. An S-bend is added before the output for filtering any residual TM0 mode present in the input waveguide. Tapering the DC helps maintain phase matching for broadband operation and increases the tolerance toward fabrication errors. The measurement shows low insertion loss (IL < 0.44 dB), high extinction ratio (ER > 15 dB), and wide bandwidth (BW = 80 nm). The overall device length is only 13 μm. A high performing TE-pass polarizer (IL < 0.89, ER > 30, and BW = 100 nm) is also demonstrated by cascading two proposed polarizers.

https://doi.org/10.1364/OL.457260

A silicon-on-insulator (SOI) platform for implementing photonic integrated circuits (PICs) is popular due to its compatibility with complementary metal-oxide semiconductor (CMOS) processes [1], which facilitate low-cost high-volume fabrication. The SOI platform offers a large refractive index contrast which causes strong optical confinement in the silicon waveguide and thus facilitates ultra-compact devices and circuits. However, due to the same reason, the polarization dispersion is also significant in the silicon waveguides [2]. In most planar waveguide cross sections, the fundamental modes (TE and TM) have different effective and group indices, mode profiles, and confinement factors. Therefore, it is challenging to design silicon photonic devices that can function for both TE and TM fundamental modes. Any fractions of unwanted cross-polarization may cause severe performance degradations in silicon photonic devices and circuits [3].

A single-mode fiber supports both the fundamental TE and TM modes and can introduce cross-polarization into the circuit. Such a situation occurs when light is coupled into the silicon chip using edge coupler (nano inverse taper) based spot-size converters. An edge coupler based on inverse taper couples both the polarization states of the fiber. Therefore, cross-polarization can be introduced to the chip. Efficient external control of polarization is required to block an unwanted polarization state. The efficiency of polarization control is not a concern when fiber grating couplers are used to couple the light. Grating couplers independently act as polarizers allowing only one state of light to couple to the chip. However, grating couplers have limited bandwidth and cannot be used universally with PICs. In addition to fiber coupling with edge couplers, cross-polarization can also occur in polarization diversity devices such as polarization rotators and polarization beam splitters with imperfect rotation [4–7]. In both cases, an on-chip polarizer is greatly desired to block cross-polarization, thus improving the performance.

The key features in a high-performing polarizer are low insertion loss (IL), high extinction ratio (ER), fabrication robustness, and compact footprint. Since CMOS compatibility is a key merit of silicon photonics, it is highly advantageous that polarizers are designed using CMOS compatible materials and processes. In the literature, many different TE-pass and TM-pass polarizers are demonstrated using the concepts of the subwavelength grating (SWG) [8], photonic crystal [9,10], hybrid silicon plasmonic [11,12], graphene [13], and asymmetric directional coupler (ADC) [14]. However, the fabrication of SWG structures and photonic crystals is challenging. The minimum feature size required by SWGs is not compatible with 193-nm deep ultraviolet (DUV) lithography. Due to scattering in the grating, the polarizers with SWG structures have high IL. Similarly, photonic crystal-based polarizers are reported to suffer from high losses. With a plasmonic waveguide, polarizers can be realized in a compact footprint. Nevertheless, the IL is still significant, and plasmonic structures require specific metals. Though the fabrication of ADC-based polarizers is simple, it has limited bandwidth (~30 nm) due to the wavelength sensitivity of the conventional directional coupler (DC). Furthermore, any fabrication error introduces phase mismatching, resulting in deviations in the designed coupling wavelength.

A tapered DC is an efficient design that relaxes fabrication tolerance and bandwidth limitation of conventional DCs and has been implemented in devices such as polarization splitters and rotators, mode multiplexers, and 3-dB couplers [15–19]. In this work, we demonstrate the first TE-pass polarizer based on a tapered DC. Furthermore, we have added a combination of S-bend and 180-degree bend for improving the ER. Overall,

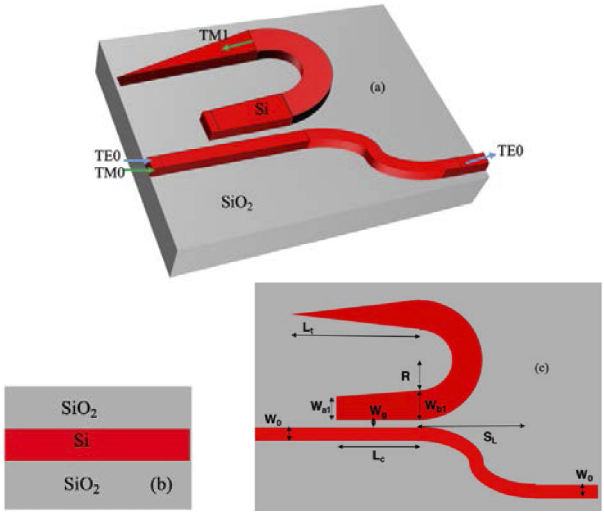

Fig. 1. (a) 3D view of TE-pass polarizer (top oxide not shown). (b) Cross section of silicon waveguide. (c) 2D schematic of TE-pass polarizer with key design parameters.

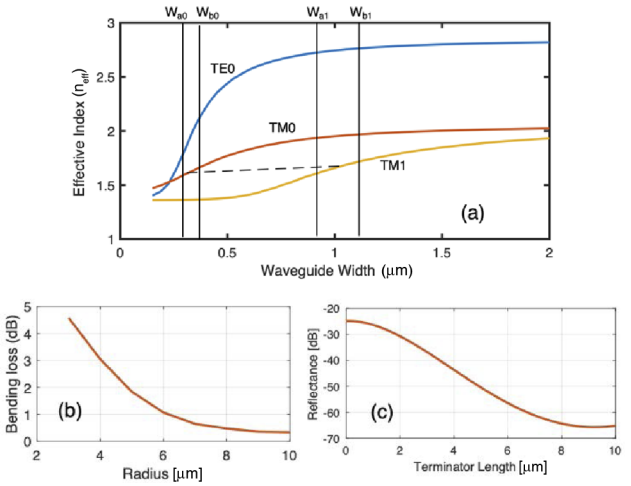

Fig. 2. (a) Calculated effective refractive indices (n_{eff}) of eigen modes versus waveguide width. (b) Bending loss as a function of radius R. (c) Reflectance versus terminator length L_t.

the proposed device has state-of-the-art performance considering fabrication robustness and CMOS compatibility on active platforms (it does not require air cladding or sub wavelength gating/photonic crystal structures). A high-performing polarizer is also demonstrated by cascading two tapered TE-pass polarizers.

The proposed TE-pass polarizer is depicted in Fig. 1. As shown in Fig. 1(b), the design is based on an SOI platform with silicon waveguide thickness of 220 nm, box oxide of 2 μm, and top cladding oxide of 2.2 μm. The TE-pass polarizer consists of an input waveguide (W_0 width) and a multimode waveguide tapered from W_{a1} to W_{b1}. The coupling gap and length are W_g and L_c, respectively. A 180-degree bend follows the multimode waveguide (radius R) and is terminated with a linear taper (length L_t). The linear taper is referred to as the 'terminator' in the rest of the manuscript. In contrast, the input waveguide is followed by an S-bend with radius r, routing the TE0 mode to the output port.

The operation of the proposed TE-pass polarizer relies on the phase-matching principle of the DC coupler. The unwanted TM0 mode in the input waveguide is coupled to the TM1 mode in the multimode waveguide. Such TM0–TM1 coupling is based on satisfying the phase-matching condition between the waveguides in a conventional DC. However, fabrication errors and wavelength deviations can easily destroy this condition. A fabrication-induced width deviation error of Δw will result in a more significant effective refractive index deviation Δn_{eff}, as shown in Fig. 2(a). A larger slope difference of Δn_{eff} will make it easier for the phase-matching condition to be destroyed. To overcome the limitations of fabrication and wavelength sensitivity, the width of the wide waveguide is tapered in the proposed design. Tapering the multimode waveguide from W_{a1} to W_{b1} will result in a width deviation tolerance of the narrow waveguide between W_{a0} and W_{b0} [Fig. 2(a)] . Hence, a phase-matching position can always be established along the tapered section of the DC.

Consequently, tapering the multimode waveguide will also increase the wavelength window for which the phase-matching condition is satisfied. The excited TM1 mode is channeled away from the input waveguide using a low-loss 180-degree bend and scattered in the terminator section. Furthermore, an S-bend is added to the input waveguide after the coupling region which offers some filtering (~10%) for any uncoupled TM0 mode and mainly prevents any back coupling to the bar waveguide. However, the launched TE0 mode will pass through the coupling section uncoupled to the tapered waveguide due to phase mismatch. The S-bend is lossless for the TE0 mode. In this way, the proposed device acts as a TE-pass polarizer allowing only the TE0 mode and blocking the unwanted TM0 mode.

Figure 2(a) shows the calculated effective indices (n_{eff}) of the eigenmodes in the SOI waveguide as a function of the waveguide width. The width of the input single-mode waveguide is chosen to be $W_0 = 400$ nm. The width of the multimode waveguide is then determined as $W_1 = 1075$ nm according to the phase-matching condition. In our proposed design, the multimode waveguide is tapered from $W_{a1} = 980$ nm to $W_{b1} = 1170$ nm. The ±95 nm width variation around 1075 nm ensures tolerance to any deviation in width. The resulting coupling length is $L_c = 5$ μm.

The transmission of the TM1 mode is turned using a 180° bend and finally converted to radiation modes in the terminator section. The loss calculation with respect to the radius (R) is shown in Fig. 2(b). The bending region is very close to the input waveguide, and selecting a very sharp bend can excite higher order modes which might phase match and couple (cross coupling) to the narrow waveguide. To avoid this problem, the TM1 mode is radiated far away from the narrow waveguide in the terminator section. Therefore, a radius R = 6 μm is selected, which gives the best trade-off between loss and footprint. The terminator length is optimized to minimize reflection, and a length $L_t = 8$ μm is selected [Fig. 2(c)]. For the guided TE0 mode, an S-bend with radius $r = 5$ μm and length $S_L = 7$ μm is added in the propagating section of the device. This further enhances the ER by filtering any residual TM0 mode present in the input waveguide. The total length of the designed structure is $Ltotal = Lc + SL = 13$ μm.

Finite-difference time-domain 3D simulations (3D FDTD) were performed to obtain beam profiles of the proposed device. The simulations are done at a central wavelength of 1550 nm. Figure 3(a) shows that the input TE0 mode passes through

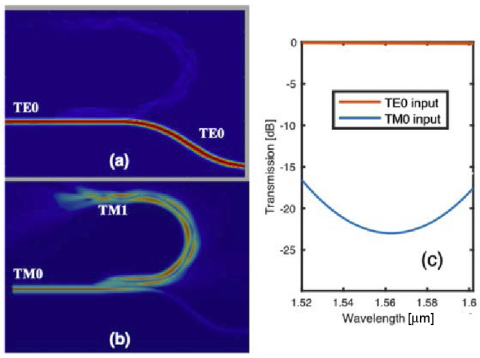

Fig. 3. (a) Beam propagation profiles with TE0 input. (b) Beam propagation profiles with TM0 input. (c) Normalized transmission spectra for TE and TM polarizations.

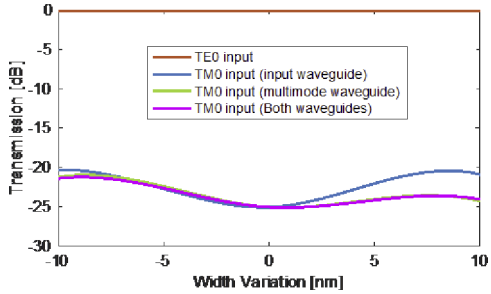

Fig. 4. Simulated transmission for TE and TM polarization input as a function of width variation.

the coupling region uncoupled and is collected at the output with negligible loss. In contrast, the input TM0 mode is efficiently coupled with the TM1 mode in the tapered multimode waveguide and scattered in the terminator region through a 180-degree bend [Fig. 3(b)]. The broadband transmission spectra are calculated using 3D FDTD and shown in Fig. 3(c). The IL for the TE mode is IL < 0.1 dB, and the ER between TE and TM modes is better than 15 dB over a wide wavelength range from 1520 nm to 1600 nm. The ER is 23 dB at the central wavelength (1550 nm).

The fabrication tolerance is also analyzed by using the 3D-FDTD simulation method. To study the effect of fabrication variability, we have considered three cases. In the first case, the width of the narrow waveguide is changed $(W_0 \pm \Delta w)$, while in the second case, the width of the wide waveguide is varied ($W_{a1} \pm \Delta w$ to $W_{b1} \pm \Delta w$). In the third case, both the narrow and wide waveguide widths are changed, where Δw is the width deviation due to fabrication error. The simulations are performed assuming a maximum process deviation in the range of ±10 nm. Figure 4 shows the calculated performance of the proposed TE-pass polarizer as a function of width deviation (Δw). For all three cases, the polarization ER is still >20 dB at the central wavelength. We have considered a constant center-to-center distance between the narrow and wide waveguides. Therefore, the gap width (W_g) between the two waveguides changes accordingly with changes in the waveguide width.

The performance can be further improved by cascading two of the proposed TE-pass polarizers. By cascading, the transmission bands of the polarizers are multiplied. The beam propagation profiles [Figs. 5(a), 5(b)] and the transmission response [Fig. 5(c)] for the cascaded polarizer (2-stage) are calculated

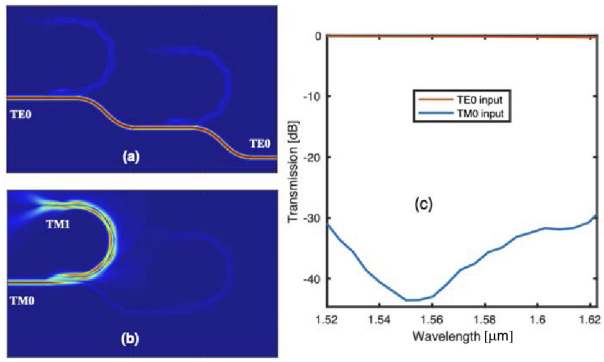

Fig. 5. (a) Beam profile of cascaded design with TE0 input (1550 nm). (b) Beam profile of cascaded design with TM0 input (1550 nm). (c) Normalized transmission spectra for the cascaded structure.

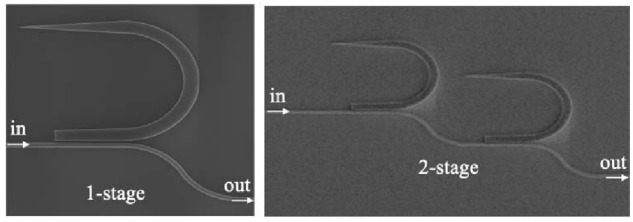

Fig. 6. SEM images of the fabricated TE-pass polarizers.

using 3D FDTD. The ER is greatly enhanced as the residual TM mode is successfully filtered out. The ER at central wavelength is ER = 43.5 dB for the 2-stage structure. Furthermore, over a 100-nm bandwidth covering the1520–1620-nm wavelength range, an ER > 30 dB and IL < 0.26 dB are achieved.

The designed TE-pass polarizers are fabricated using the NanoSOI fabrication process by Applied Nanotools Inc., based on direct-write 100-keV electron beam lithography technology. Scanning electron microscopy (SEM) micrographs of the fabricated device are shown in Fig. 6. A Keysight 81600B tunable laser was used as a source, and an external polarization controller was used for switching between TE0 and TM0 modes. The light was edge coupled from a lensed fiber into the silicon chip, through an inverse taper-based spot size converter. A Keysight N7744A optical detector sensor measured the device wavelength response.

Figure 7 shows the measured normalized transmission spectra for the polarizers. The transmission spectra in Fig. 7 are normalized with respect to a straight waveguide without any devices to account for input/output coupling loss of the edge couplers. From the spectra, the measured IL and ER at 1550 nm are IL = 0.2 dB, ER = 20 dB for the 1-stage device, respectively. The corresponding values for a 2-stage device are IL = 0.52 dB and ER = 33 dB. For the 1-stage polarizer, over a bandwidth of 80 nm from 1520 to 1600 nm, the IL is less than 0.44 dB with an ER better than 15 dB. In comparison, the 2-stage polarizer has a bandwidth of 100 nm with IL< 0.89 dB and ER > 30 dB.

The increase in IL for both the polarizers is due to fabrication imperfections and the accuracy of the measurement setup. Here we are reporting the peak value (maximum) of IL in a broad wavelength range. As the IL is wavelength dependent, the fabrication imperfection may cause the peak loss to shift. In addition, measurement setup errors are more pronounced when reporting

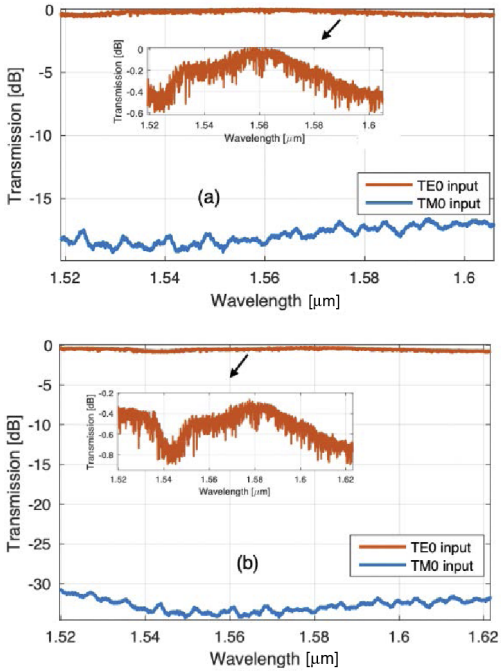

Fig. 7. Measured normalized transmission spectra of the proposed TE-pass polarizer: (a) 1-stage; (b) 2-stage.

Table 1. Comparison of On-chip Polarizers

Waveguide Structure	Footprint/ μm	IL/dB	ER/dB	BW/nm
SWG [8]	9	<1	20	60
Photonic crystals [9]	4	1	>30	>50
Nano plasmonic [11]	1	2.2	16	80
Hybrid plasmonic [12]	30	2–3	23–28	60
Graphene [13]	4000	9	27	>80
ADC [14]	29.39	1.04	15	>80
Tapered ADC [This work]	13	<0.45	>15	>80
2-stage tapered ADC [This work]	29	<0.89	>30	>100

the peak value. The sidewall roughness will have a minimal impact on increasing the loss profile due to scattering. Furthermore, dimensional variations in the waveguide width cause the ER to be lower, which matches our tolerance simulation. In the case of the 2-stage polarizer, the difference is higher due to the limited polarization ER of our setup [~35 dB].

The device length is only 13 and 29 for the 1-stage and 2-stage polarizer structures, respectively. Table 1 summarizes performance matrices of reported on-chip polarizers. As shown in the comparison of Table 1, our demonstrated tapered DC-based polarizers exhibit low losses, wideband operation, and a high ER with compact footprints. The minimum feature size (200 nm) is fully compatible with 193-nm DUV.

We have demonstrated high-performance, fabrication tolerant, and novel TE-pass polarizers using a tapered DC on an SOI platform. The single-stage polarizer is measured to have an IL < 0.44 dB and an ER > 15 dB over a 1520–1600 nm wavelength range. An ER > 30 dB with IL < 0.89 dB over a bandwidth > 100 nm is experimentally achieved by cascading two proposed polarizers. The footprint of the 2-stage polarizer is still compact (~29 μm) compared to most of the reported devices.

Acknowledgment. This research was in part performed by using the Core Technology Platform (CTP) resources at NYUAD. Simulations for this research were partially carried out on the High-Performance Computing resources at NYUAD.

Disclosures. The authors declare no conflicts of interest.

Data availability. The data underlying the results presented in this Letter are not publicly available at this time but may be obtained from the authors upon reasonable request.

REFERENCES

1. R. Soref, IEEE J. Sel. Top. Quantum Electron. **12**, 1678 (2006).
2. Z. Mohammed, B. Paredes, and M. Rasras, Appl. Sci. **11**, 2366 (2021).
3. H. Fukuda, K. Yamada, T. Tsuchizawa, T. Watanabe, H. Shinojima, and S. Itabashi, Opt. Express **16**, 4872 (2008).
4. D. Dai and H. Wu, Opt. Lett. **41**, 2346 (2016).
5. W. D. Sacher, T. Barwicz, B. J. F. Taylor, and J. K. S. Poon, Opt. Express **22**, 3777 (2014).
6. D. Dai and J. E. Bowers, Nanophotonics **3**, 283 (2014).
7. D. Dai, L. Liu, S. Gao, D.-X. Xu, and S. He, Laser Photonics Rev. **7**, 303 (2013).
8. X. Guan, P. Chen, S. Chen, P. Xu, Y. Shi, and D. Dai, Opt. Lett. **39**, 4514 (2014).
9. D. W. Kim, M. H. Lee, Y. Kim, and K. H. Kim, Opt. Express **24**, 21560 (2016).
10. Y. Cui, Q. Wu, E. Schonbrun, M. Tinker, J.-B. Lee, and W. Park, in *2007 7th IEEE Conference on Nanotechnology (IEEE NANO)* (2007), pp. 1093–1096.
11. Y. Huang, S. Zhu, H. Zhang, T.-Y. Liow, and G.-Q. Lo, Opt. Express **21**, 12790 (2013).
12. X. Sun, M. Z. Alam, S. J. Wagner, J. S. Aitchison, and M. Mojahedi, Opt. Lett. **37**, 4814 (2012).
13. C. Pei, L. Yang, G. Wang, Y. Wang, X. Jiang, Y. Hao, Y. Li, and J. Yang, IEEE Photonics Technol. Lett. **27**, 927 (2015).
14. H. Xu and Y. Shi, IEEE Photonics Technol. Lett. **29**, 861 (2017).
15. Y. Ding, J. Xu, F. D. Ros, B. Huang, H. Ou, and C. Peucheret, Opt. Express **21**, 10376 (2013).
16. Y. Ding, L. Liu, C. Peucheret, and H. Ou, Opt. Express **20**, 20021 (2012).
17. Y. Luo, Y. Yu, M. Ye, C. Sun, and X. Zhang, Sci. Rep. **6**, 23516 (2016).
18. B. Paredes, Z. Mohammed, J. Villegas, and M. Rasras, IEEE Photonics J. **13**, 1 (2021).
19. B. Paredes, Z. Mohammed, J. Villegas, and M. Rasras, in *2021 Optical Fiber Communications Conference and Exhibition (OFC)* (2021), pp. 1–3.